

# Structural elements of CeO<sub>2</sub>(111) surfaces

S Gritschneider and M Reichling

Fachbereich Physik, Universität Osnabrück, BarbarasträÙe 7, 49076 Osnabrück, Germany

E-mail: [reichling@uos.de](mailto:reichling@uos.de)

Received 25 October 2006, in final form 4 December 2006

Published 21 December 2006

Online at [stacks.iop.org/Nano/18/044024](http://stacks.iop.org/Nano/18/044024)

## Abstract

The atomic structure of the CeO<sub>2</sub>(111) surface in different states of cleanliness and reduction is studied in an ultra-high vacuum with high resolution dynamic scanning force microscopy operated in the non-contact mode (nc-AFM) and its structural elements are described by their characteristic contrast patterns. From a synopsis of results we develop a self-consistent interpretation of contrast features that is cross-checked by a systematic variation of experimental conditions and a comparison to previously obtained results. The most common deviations from the regular structure of the stoichiometric surface are surface oxygen vacancies, water adsorbed on top of cerium ions and hydroxide substituting surface oxygen. All of the species are found as single defects as well as in the form of structures composed of several similar defects. We find that water readily adsorbs on the surface and forms hydroxide if oxygen vacancies are present, while both the clean and defective surfaces are rather inert against exposure to molecular oxygen.

(Some figures in this article are in colour only in the electronic version)

## 1. Introduction

Cerium dioxide (CeO<sub>2</sub>, ceria) is a material with a large variety of technical applications, many of them related to its remarkable catalytic properties [1]. The high oxygen storage capacity of ceria facilitates, for instance, its use as a three way catalyst [2]. Catalytic activity involves a gas–solid interface, and therefore the surfaces of ceria model systems have been investigated by a wide range of experiments including the study of surface reactions [3], phase transitions [4] and adsorption and desorption phenomena of various species [5, 6]. Among these experiments, studies with the force microscope are outstanding as dynamic scanning force microscopy (SFM) operated in the so-called non-contact mode (nc-AFM) is the only nanoscience tool capable of direct atomic scale imaging of insulating surfaces and nanostructures [5, 7, 8]. Principally this technique now offers the unique possibility to study chemical processes in real space at the atomic scale, for instance by imaging single (defective) surface sites in a time series during exposure to probe molecules, a capability that has formerly been restricted to scanning tunnelling microscopy studies of conducting oxides [9]. However, a prerequisite for the investigation of chemical processes is an understanding of SFM contrast formation for structures on clean and gas exposed surfaces. The purpose of the present

contribution is to provide an overview of structural elements observed on stoichiometric, slightly reduced and contaminated CeO<sub>2</sub>(111) surfaces and to develop a consistent picture of their interpretation.

Experiments reported here were performed with the same sample and the same force microscope used in our earlier studies [10]. The surface is scanned with a sharp tip mounted on a cantilever oscillating at its resonance frequency of typically 60–70 kHz (Nano World AG, PPP-QFMR). Any interaction with the surface results in a slight change in the resonance frequency, commonly referred to as the *detuning*, that is detected by a phase locked loop demodulator. The images are taken in the *constant height mode*, so that all atomic scale information is fully represented in the cantilever detuning signal [11]. To achieve optimum imaging conditions, we apply oscillation amplitudes of 25–40 nm and a scanning speed of 2–5 lines s<sup>-1</sup>. Values for average detuning strongly depend on tip conditions and are found in the range of –5 to –50 Hz. Note that in the images presented here, a bright colour corresponds to a larger negative detuning than a dark colour and, therefore, the bright colour represents enhanced attractive tip–surface interaction or a topographic elevation. To compensate for any relevant contact potential or charges present on the insulating sample surface, an appropriate bias voltage  $U_{dc}$  is applied between the tip and the metallic sample

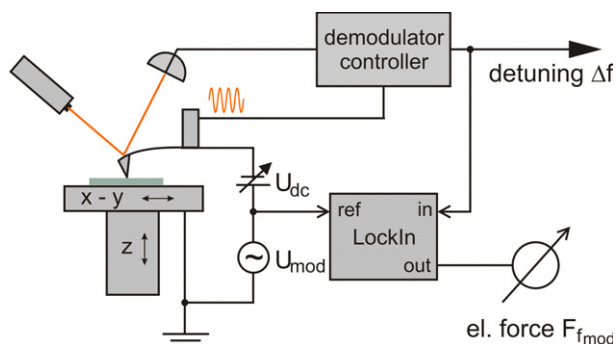


**Figure 1.** Dynamic force microscopy setup illustrating how to adjust the bias voltage  $U_{dc}$  to compensate for electrostatic forces.

support. We determine the compensating voltage  $U_{dc}$  using a setup that allows us to check for electrostatic forces without suspending the scanning process. As schematically depicted in figure 1, we add a small low frequency signal  $U_{mod}$  to  $U_{dc}$  that results in a slight modulation of the detuning  $\Delta f$  with the frequency  $f_{mod}$  (420 Hz). This additional signal is detected by a lock-in amplifier measuring the amplitude of the first harmonic component of the electrostatic force [12]. This harmonic vanishes if  $U_{dc}$  exactly matches the surface potential. Prior to each experiment we adjust  $U_{dc}$  to a minimum lock-in signal. Sample preparation includes several cycles of  $Ar^+$ -ion sputtering and subsequent annealing of the surface to 900 °C according to a recipe published elsewhere [7]. After a successful preparation, the surface exhibits stacks of atomically flat hexagonal terraces and pits. The degree of reduction of the surface and, consequently, the density of defects can be tuned by a variation of the annealing time and temperature. While we obtain a stoichiometric and well ordered surface, as shown in figure 2(a), by annealing the sample for 3 min at temperatures up to 900 °C, a defective surface is prepared by extending this period or by introducing reactive agents like water or carbon monoxide during annealing.

## 2. The stoichiometric surface

A first step in understanding the ceria surface is to understand SFM contrast formation on the stoichiometric surface. As ceria is an oxide with the fluorite structure and a lattice constant very close to that of  $CaF_2$  [13], it appears to be straightforward to transfer concepts developed for contrast formation on  $CaF_2(111)$  to  $CeO_2(111)$ . When measuring a clean  $CaF_2(111)$  surface, atomically resolved SFM measurements allow an identification of ionic sub-lattices when they are interpreted with an appropriate theoretical model [14]. It has, however, turned out that it is not at all straightforward to transfer the simple fluorite model of contrast formation to  $CeO_2(111)$ . This stems from the fact that contrast formation in dynamic SFM is a complex process involving various interactions. Depending on the detailed chemical structure, electronic states of the foremost tip atoms and a balance between the respective interactions, a variety of imaging features may be observed. In the case of  $CeO_2$ , a quantitative interpretation of contrast formation in scanning force microscopy is further hampered by the electronic structure involving 4f states that are most

difficult to model with available quantum chemical codes [15]. Due to these peculiarities, there is at present no model of contrast formation on the  $CeO_2(111)$  surface that could quantitatively explain the experimentally observed contrast features on the basis of a quantum chemical simulation.

However, a large amount of experimental evidence collected over the last years [5, 7, 8, 10] together with the present work allows us to establish a realistic description of contrast formation on  $CeO_2(111)$ . We have developed a phenomenological model of contrast formation which well explains the atomic contrast in our images and is fully supported by the reproducibility of the major contrast features and a large number of consistent findings from very different experimental situations and surface conditions. While details and a justification of this model will be communicated in a forthcoming publication [16], here we explain some basic features that are necessary to understand the results presented below.

The basic contrast feature found in most experiments is a regular hexagonal pattern of circular structures as shown in figure 2(b). The bright, disc-like spots are associated with the surface terminating oxygen layer. To explain this contrast within a concept of ionic interaction, a plausible tip model is that of an oxide tip apex that is covered by hydroxides in a way such that at least one  $OH^-$  group is the imaging cluster with the hydrogen part pointing towards the surface. In that way, the tip has a positive electrostatic potential, and accordingly the highest attraction (bright contrast) is observed above the negatively charged oxygen ions. Upon closer approach of the tip towards the surface, however, we frequently observe that the contrast pattern reversibly changes to a honeycomb like structure as shown in figure 2(c). Many experimental observations prove that this is not a contrast reversal as it is observed for  $CaF_2(111)$  where the disc-like contrast may be switched to a honeycomb-like pattern by a change in polarity of the tip-terminating ion [11]. One piece of evidence for this claim is the analysis of defects on  $CeO_2(111)$  described below where contrast formation of the defect is not influenced by a change in contrast of the underlying substrate. We attribute the contrast change to a rearrangement of tip atoms resulting in an enhanced interaction of the tip with second layer oxygen ions. Possibly, another  $OH^-$  group of the tip apex is brought into the surface force field by the tip change and adds significantly to the total tip-surface interaction. The honeycomb pattern is the result of a superposition of contributions from first and second layer oxygen ions. As illustrated in figure 2(c), the mesh of bright contrast represents the oxygen sub-lattices while the dark spots mark the cerium sub-lattice.

## 3. Vacancy structures

Oxygen vacancy defects play a key role in the surface chemistry of oxides and are the key for an understanding of hydroxylation and other surface reactions on  $CeO_2(111)$ . Figures 3 and 4 are a compilation of vacancy defect structures that are typically found on a surface prepared under slightly reducing conditions. We find that vacancy defects can appear as isolated single vacancies (figure 3(a)) or as clusters in the form of lines (panel (b)) or triangles (panels (c) and (d)). Single vacancies are a relatively rare species, and the creation of extended line defects requires special surface treatment. The

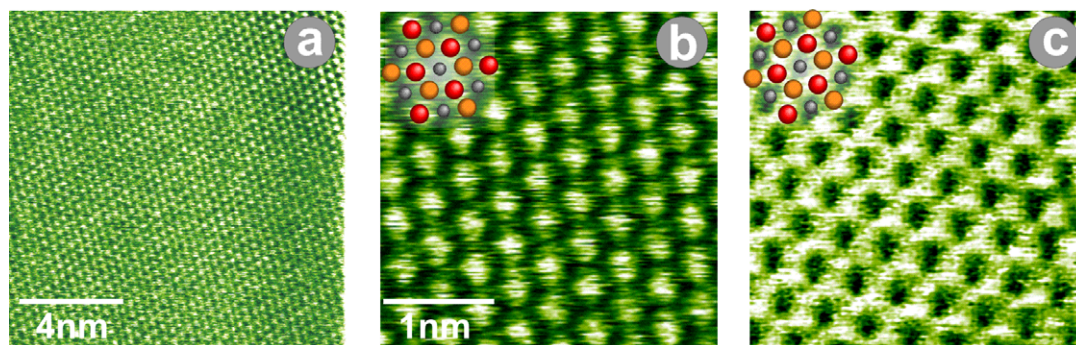


**Figure 2.** (a) Large stoichiometric terraces on  $\text{CeO}_2(111)$  exhibit perfect atomic order of the topmost oxygen layer. (b) Magnified area demonstrating a disc-like contrast pattern that is obtained for most imaging conditions. (c) Upon close approach of the tip to the surface, the contrast may turn into a bright honeycomb pattern with the dark holes representing the cerium ions. The scheme inserted in the upper left corner of panels (b) and (c) defines the position of ions in the terminating O–Ce–O triple, namely top oxygen (red), low oxygen (orange) and cerium (grey).

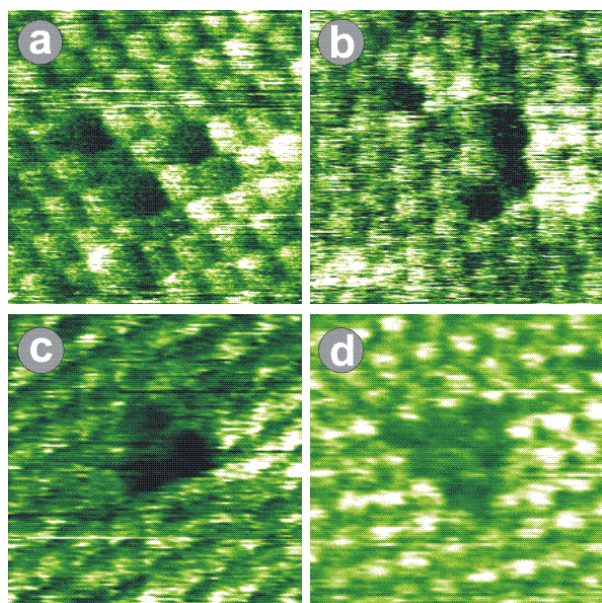


**Figure 3.** Surface vacancies appearing as (a) single vacancies, (b) in-line configurations and (c) + (d) triangular vacancy clusters.

most abundant species is clearly a triangular triple vacancy, and in a forthcoming paper we will demonstrate that such triple vacancies are very reactive and exhibit a rich variety of interactions with water [17]. A noteworthy feature of our SFM investigations is that vacancies always appear as holes sharply cut out of the lattice of surface oxygen ions, and in contrast to recent STM investigations [18] we do not observe any relaxation of neighbouring ions. Figure 4(a) is a clear demonstration of this finding for the example of a double vacancy where both the circular features representing oxygen ions as well as the dark circles representing the vacancies are of exceptional regularity. The bright contrast feature adjacent to the double vacancy is clearly a scanning artefact, as the bright feature changes position upon a reversal of the scanning direction.

Figures 4(b) and (c) show two further frequently observed vacancy configurations that we interpret as combinations of vacancies with adsorbates. The species shown in panel (b) is a double vacancy with an adjacent hydroxide (marked by

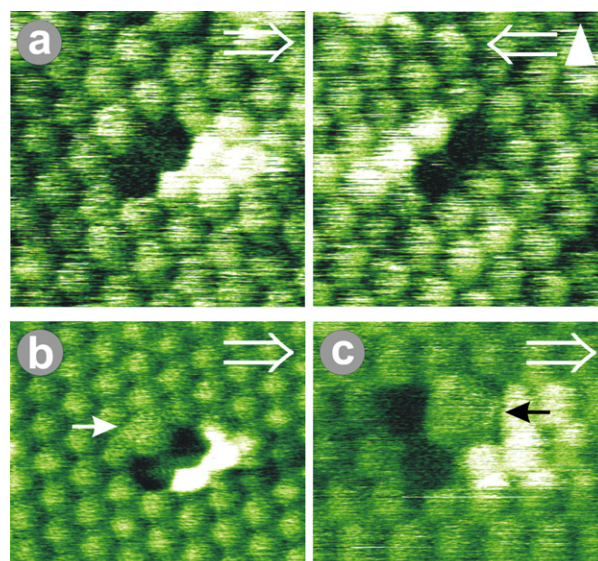


**Figure 4.** (a) A double vacancy recorded in forward ( $\Rightarrow$ ) and backward ( $\Leftarrow$ ) direction. No relaxation of the surrounding oxygen ions is observed. The white features that appear in the scanning direction behind the defects are an experimental artefact due to the slow topography feedback settings. (b) A double vacancy with an attached hydroxide (white arrow). (c) A double vacancy with an attached water molecule (black arrow).

the white arrow), the latter identified by the enhanced circular contrast feature on an oxygen site. As this structure frequently occurs on slightly reduced surfaces exposed to water, we speculate that it originates from a water molecule dissociated at a triple vacancy where the remaining hydroxide after the reaction occupies one of the vacancy sites. In the same sense, the configuration shown in panel (c) is interpreted as a triple vacancy acting as a trap for a water molecule (marked by the black arrow). Interestingly, this is also a frequent configuration, suggesting that water is not necessarily dissociated when in contact with a vacancy cluster.

#### 4. Water related structures

In figures 5 and 6 we show results from slightly reduced surfaces exposed to water. Apparently, vacancies created under

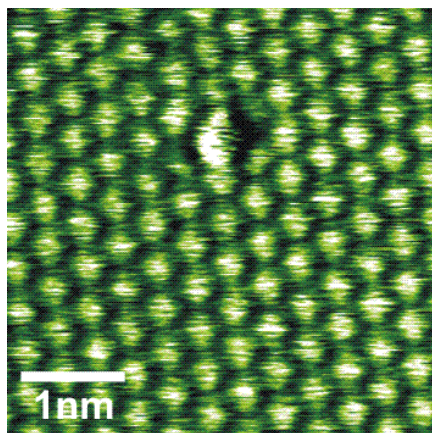


**Figure 5.** A single hydroxide on a stoichiometric terrace. The black shadow at the right side of the hydroxide partly covering the surrounding surface oxygen ions is a scanning artefact.

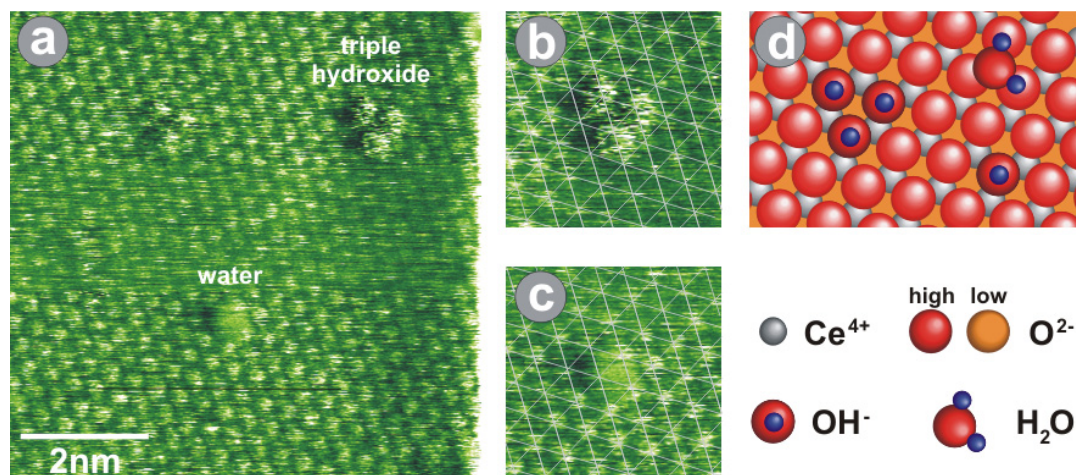
reducing conditions can act as centres of water dissociation and are converted to hydroxide substituting for surface oxygen. Very rarely we observe a single hydroxide, such as the one shown in figure 5. A characteristic SFM contrast feature of hydroxide is a slight imaging instability at the location of the defect so that the hydroxide appears as an enlarged bright spot at an oxygen lattice site with an enhanced stripe pattern in the fast scanning direction. This could be caused by an increased interaction between the tip and the hydrogen adatom of the hydroxide; however, it is unclear at present why such a phenomenon is not observed for adsorbed water. We speculate that this is due to the different binding of the species to the surface and their different structure. While a water molecule is physisorbed on the surface and its two hydrogens can easily be rotated and distorted they produce a smoother contrast than a hydroxide that is firmly embedded into the surface. To demonstrate how clearly adsorbed water can be discriminated from hydroxide species, we show in figure 6 a situation where water is found close to hydroxide. In this image, hydroxide appears in the form of triples, which is, in fact, the most frequently observed stable hydroxide species that well corresponds to the frequent appearance of triple vacancies described in section 3. Figures 6(b) and (c) are enlarged areas from panel (a) where we analyse the position of water related defects with respect to the ionic lattice of the substrate. We superimposed a  $(1 \times 1)$  mesh with crossing points centred at the positions of surface oxygen ions. As is discussed in detail in [19], the water molecule (panel (c)) is centred at a hollow position in between three surface oxygen ions and the hydroxides of the triple cluster (panel (b)) are clearly located at crossings of the grid confirming that they substitute for surface oxygen. Figures 6(b) and (c) also clearly demonstrate the difference in apparent contrast between water and hydroxide. While the former species is a somewhat fuzzy triangular feature that appears smoother than the surrounding oxygens, the latter exhibits three clearly distinguished sub-units and the stripe contrast of slight instability.

Figure 7(a) shows a stoichiometric surface exhibiting a honeycomb type contrast (see section 2) after exposure to 1.7 L of water. Such a dosage experiment yields evidence that the protrusion defects are indeed created by adsorption

of water. The coverage of protrusion defects apparent in figure 7(a) has been created at a water partial pressure of  $1.5 \times 10^{-6}$  Pa within a period of 150 s, while it takes more than 6 h to create a similar coverage by exposure to the residual gas at a typical base pressure of  $1.0 \times 10^{-8}$  Pa. This image corroborates our interpretation of honeycomb contrast formation and the magnified panel in figure 7(b) allows an unambiguous determination of the adsorption site of the water molecule. For comparison we have depicted an equivalently contaminated surface area that is imaged with disc-like contrast in figure 7(d). Note that the apparent contrast of adsorbed water as a protruding defect is very similar for both contrast patterns and there is no indication of any type of contrast inversion of the water molecules. However, water molecules appear somewhat flattened in panel (a), maybe due to the smaller tip-sample distance that is also responsible for the formation of the honeycomb contrast. As water is a rather soft material that is easily deformed, its appearance in a force microscopy image does not depend critically on the atomic details of the probing tip. Figures 7(b) and (c) represent an enlarged region from panel (a) with and without a superimposed grid whose crossing points are here centred at the cerium sub-lattice. In this way we can unambiguously determine the exact position of the centre points of the individual water features with respect to the subjacent ionic grid. All molecules are located at the crossing points of the  $(1 \times 1)$  mesh representing cerium sites which is in excellent agreement with the enlarged images shown in figures 7(e) and (f), where the grid is centred on the oxygen ions and the molecules appear at hollow positions that represent again cerium lattice sites.

## 5. Survey and summary

Our methods of sample preparation allow us to create  $\text{CeO}_2(111)$  surfaces with very large stoichiometric and clean terraces, as well as to intentionally create a defective or water covered surface. Room temperature scanning force microscopy measurements provide not only structural information on the stoichiometric surface with flat terraces and step edges but also allow a detailed characterization of various types of vacancy defects as well as adsorbates and reaction products when the surface is exposed to water. Atomic contrast features on clean, stoichiometric surfaces represent the sub-lattice of topmost oxygen ions where vacancies appear as empty oxygen sites, as one would expect intuitively. When no special precautions are taken to yield a specific preparation result, the freshly prepared surface exhibits a combination of defects and adsorbates as well as reaction products that stem from the interaction of surface defects with the residual gas. Figure 8(a) provides a survey of such a surface prepared under conditions where the most abundant species are water molecules. From this and similar images, we conclude that the room temperature mobility of all observed species is small as, except for water adsorption events, we hardly observe any change in a repetitively scanned image. Figures 8(b)–(f) show details highlighting the major surface irregularities. On the right-hand side of the two water molecules apparent in panel (b), we find a single oxygen vacancy (marked by a white arrow) that appears as a clearly cut hole instead of an oxygen ion. The result shown in panel (c) demonstrates that vacancies and water



**Figure 6.** (a) Two triple hydroxide clusters and a water molecule at a stoichiometric terrace. (b) Each hydroxide of the triple cluster is located at an oxygen position. (c) The water molecule adsorbs at threefold hollow sites. The superimposed ( $1 \times 1$ ) mesh marks oxygen positions by the crossing points of the lines. (d) Surface model illustrating the geometry of hydroxide, triple hydroxide and water molecules.

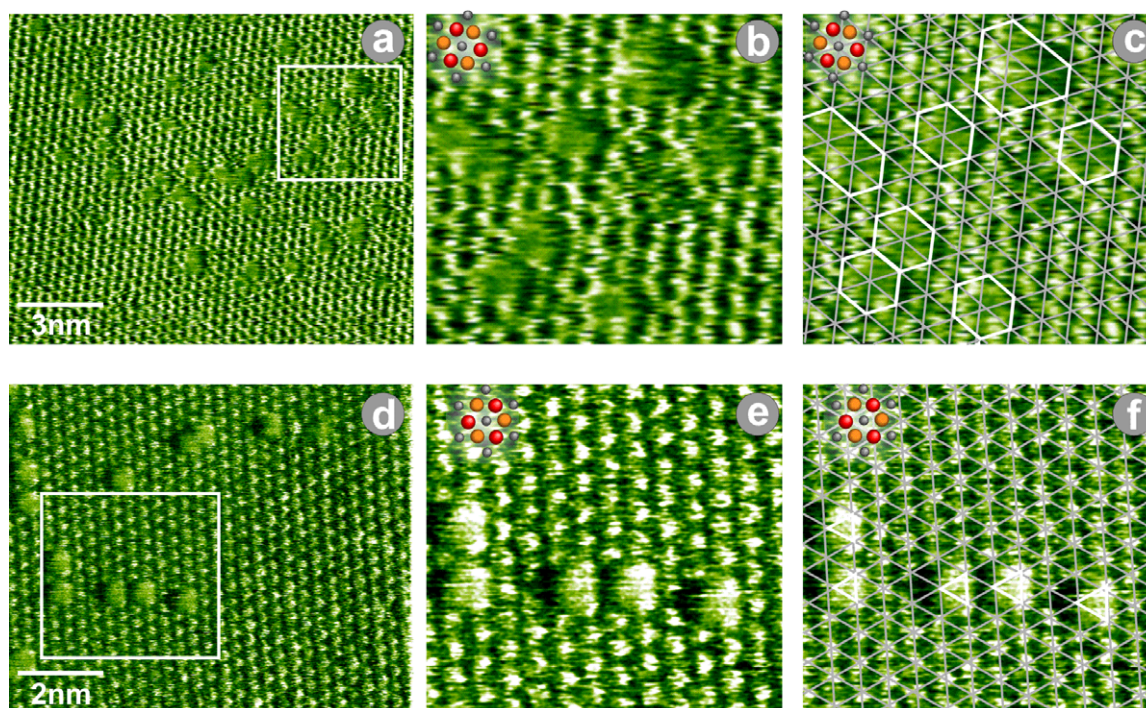


**Figure 7.** (a) Stoichiometric  $\text{CeO}_2(111)$  surface exhibiting honeycomb type contrast and covered with water molecules. (b) Detail taken from the rectangular area of panel (a). (c) The same area shown with a superimposed grid (light grey) with its crossing points defining the cerium sub-lattice. Protrusions framed by white hexagons are adsorbed water molecules. In panels (d) to (f), an equivalent surface area exhibiting disc-like contrast is shown for direct comparison. Here, the crossing points of the superimposed grid defines the oxygen sub-lattice. The scheme inserted in the upper left corner of panels (b), (c), (e) and (f) defines the position of ions in the terminating O–Ce–O triple, namely top oxygen (red), low oxygen (orange) and cerium (grey).

molecules may coexist even in very close proximity. In panel (c) two vacancies are connected by a bridge formed by two water molecules. The structure shown in panel (d) is the least well understood at present. The image shows an apparently stoichiometric surface region, but a group of surface ions appears with an enhanced contrast. The contrast enhancement is, however, distributed unevenly over the respective surface sites and the individual contrast features are distinctly different from that of a hydroxide. Hence, we do not interpret them as

hydroxide clusters but tentatively regard the feature as a surface relaxation effect induced by sub-surface defects or impurities. Products of surface reactions are highlighted in panels (e) and (f) where we find protrusions located at oxygen sites (marked by white arrows) that are clearly identified as single and triple hydroxide species, respectively.

The synopsis of investigations reviewed here provides evidence for surface vacancies, water, hydroxide and a large number of surface structures created by a combination of

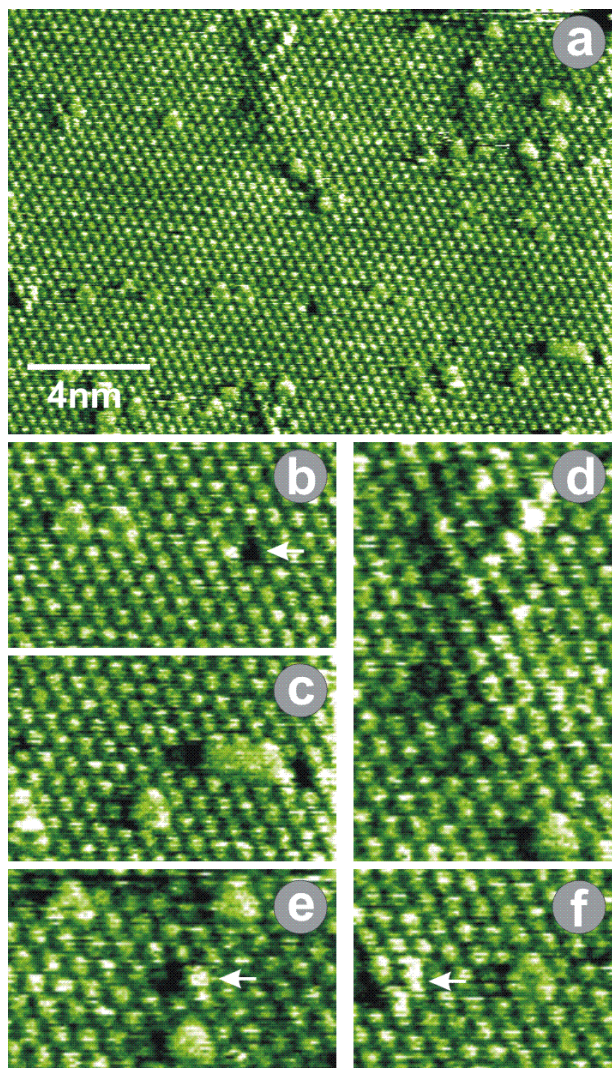


**Figure 8.** (a) A surface prepared under typical conditions after several hours of experiment exhibits a coexistence of various defects. (b)–(f) Enlarged regions extracted from (a) representing frequently observed defect structures. (b) Protruding defects located on threefold hollow sites are identified as water molecules. They are easily distinguished by their characteristic triangular appearance. An oxygen vacancy, marked by the small white arrow, appears as a hole at an oxygen site. (c) Water molecules may coexist with vacancies even in very close proximity. (d) An extended region with inhomogeneous contrast speculatively assigned to sub-surface defects or impurities. (e) Hydroxide replacing a surface oxygen ion appears as a larger protrusion at an oxygen position. (f) Triple hydroxides are found to form stable triangles.

these three basic features on a  $\text{CeO}_2(111)$  surface prepared under ultra-high vacuum conditions. Based solely on our experimental findings, we develop an interpretation for the contrast features observed in dynamic force microscopy that is self-consistent and perfectly describes a large number of detailed results of our experiments and previous studies that cover a large range of experimental conditions. Having

identified the fundamental structures on this surface, it will be a challenging task to study the reactions leading to their formation and to uncover surface processes that may be relevant for oxygen storage and catalytic activity of ceria.

## Acknowledgments

This work was supported by the single molecule program of the Stiftung Volkswagenwerk and the Deutsche Forschungsgemeinschaft. We are most grateful to Y Iwasawa for providing the sample and preparation recipe used in the present work and for stimulating discussions about  $\text{CeO}_2$  surface chemistry. Contributions to discussions from F Esch, A Foster, A Shluger, S Torbrügge and M Watkins are gratefully acknowledged.

## References

- [1] Trovarelli A, de Leitenburg C, Boaro M and Dolcetti G 1999 *Catal. Today* **50** 353
- [2] Bernal S, Kaspar J and Trovarelli A 1999 *Catal. Today* **50** 173
- [3] Yao H C and Yao Y F Y 1984 *J. Catal.* **86** 254
- [4] Gandhi H S, Graham G W and McCabe R W 2003 *J. Catal.* **216** 433
- [5] Henderson M A, Perkins C L, Engelhard M H, Thevuthasan S and Peden C H F 2003 *Surf. Sci.* **526** 1
- [6] Al-Madfa H A, Khader M M and Morris M A 2004 *Int. J. Chem. Kin.* **36** 293
- [7] Pushkarev V V, Kovalchuk V I and d'Itri J L 2004 *J. Phys. Chem. B* **108** 5341
- [8] Xiao W D, Guo Q L and Wang E G 2003 *Chem. Phys. Lett.* **368** 527
- [9] Namai Y, Fukui K-i and Iwasawa Y 2004 *Nanotechnology* **15** S49
- [10] Luo M F, Zhong Y J, Zhu B, Yuan X X and Zheng X M 1997 *Appl. Surf. Sci.* **115** 185
- [11] Bulanin K M, Lavalley J C, Lamotte J, Mariey L, Tsyganenko N M and Tsyganenko A A 1998 *J. Phys. Chem. B* **102** 6809
- [12] Fukui K-I, Namai Y and Iwasawa Y 2002 *Appl. Surf. Sci.* **188** 252
- [13] Namai Y, Fukui K-I and Iwasawa Y 2003 *J. Phys. Chem. B* **107** 11666
- [14] Wendt S, Matthesen J, Schaub R, Vestergaard E K, Laegsgaard E, Besenbacher F and Hammer B 2006 *Phys. Rev. Lett.* **96** 066107
- [15] Gritschneider S, Namai Y, Iwasawa Y and Reichling M 2005 *Nanotechnology* **16** S41
- [16] Barth C, Foster A S, Reichling M and Shluger A L 2001 *J. Phys.: Condens. Matter* **13** 2061
- [17] Zerweck U, Loppacher C, Otto T, Grafstrom S and Eng L M 2005 *Phys. Rev. B* **71** 125424
- [18] Lide D R 1992 *CRC Handbook of Chemistry and Physics* 72nd edn (Boca Raton, FL: CRC Press)
- [19] Foster A S, Barth C, Shluger A L and Reichling M 2001 *Phys. Rev. Lett.* **86** 2373
- [20] Hofer W A, Foster A S and Shluger A L 2003 *Rev. Mod. Phys.* **75** 1287
- [21] Gritschneider S and Reichling M 2007 in preparation
- [22] Gritschneider S, Iwasawa Y and Reichling M 2007 in preparation
- [23] Esch F, Fabris S, Zhou L, Montini T, Africh C, Fornasiero P, Comelli G and Rosei R 2005 *Science* **309** 752
- [24] Gritschneider S, Iwasawa Y and Reichling M 2007 *Nanotechnology* **18** 044025